# Hg 0 removal from simulated flue gas over CeO 2/HZSM-5

**ARTICLE** *in* ENERGY & FUELS · MARCH 2012

Impact Factor: 2.79 · DOI: 10.1021/ef201739p



**8 AUTHORS**, INCLUDING:

Caiting Li
Hunan University
**88** PUBLICATIONS **561** CITATIONS
SEE PROFILE

Pei Lu
Chinese Academy of Sciences
**38** PUBLICATIONS **247** CITATIONS
SEE PROFILE

energy&fuels

Article

pubs.acs.org/EF

# $Hg^0$ Removal from Simulated Flue Gas over $CeO_2$/HZSM-5

Xiaopeng Fan, Caiting Li,* Guangming Zeng, Xing Zhang, Shasha Tao, Pei Lu, Ya Tan, and Diqiang Luo

College of Environmental Science and Engineering, and Key Laboratory of Environmental Biology and Pollution Control (Ministry of Education), Hunan University, Changsha 410082, People's Republic of China

**ABSTRACT:** The effects of zeolite (HZSM-5 was chosen for use) modified by $CeO_2$ ($CeO_2$/HZSM-5) on the gas-phase elemental mercury ($Hg^0$) removal were investigated under simulated flue gas. The Brunauer−Emmett−Teller surface area analyses, powder X-ray diffraction measurements, and thermogravimetric analyses were employed to characterize the samples. The experimental results showed that there was a synergetic effect between $CeO_2$ and HZSM-5 on $Hg^0$ removal. The acidic sites of HZSM-5 could effectively adsorb $Hg^0$ from the flue gas, and $CeO_2$ could significantly enhance the oxidation of adsorbed $Hg^0$. However, the surface area of $CeO_2$/HZSM-5 decreased because of excess $CeO_2$, which was detrimental to its $Hg^0$ removal efficiency. Moreover, the temperature tests manifested that 6% $CeO_2$/HZSM-5 achieved high $Hg^0$ removal efficiency at low reaction temperatures (<300 °C). Additionally, the $Hg^0$ removal efficiencies of $CeO_2$/HZSM-5 were found to be significantly affected by the flue gas components. In the presence of $O_2$, promotional effects of NO and $SO_2$ on the $Hg^0$ removal were found, while the presence of $H_2O$ inhibited the $Hg^0$ removal in this experiment. Furthermore, after regeneration, $CeO_2$/HZSM-5 still possessed good reactivity and its $Hg^0$ removal efficiency stayed above 92% in 30 h.

## 1. INTRODUCTION

Mercury can be released into the atmosphere easily because of its extremely high volatility. It will then deposit into rivers, lakes, and oceans, producing the most toxic species of mercury, methylmercury, which can bioaccumulate within living organisms from the food chain and cause adverse effects on human health.[1−4] According to reports, the mercury emissions from coal-fired plants account for approximately one-third of the anthropogenic mercury emissions.[5,6] Thus, development of technologies governing/controlling the mercury emissions from coal-fired power plants has become an urgent issue.

Mercury in coal-fired flue gas is often presented as element mercury ($Hg^0$), oxidized mercury ($Hg^{2+}$), and particle-bound mercury ($Hg^p$).[7] As reported, different species of mercury have different physical and chemical properties.[8] $Hg^{2+}$ is soluble in water and has the tendency to associate with particulate matter. Hence, $Hg^p$ and $Hg^{2+}$ can be removed by air pollution control devices, such as electrostatic precipitators (ESPs) or scrubbers. However, most $Hg^0$ are hardly captured by these devices because of its low melting point (−38.9 °C), high equilibrium vapor pressure (0.25 Pa at 25 °C), and low solubility in water (60 mg/m$^3$ at 25 °C). Therefore, with consideration of the properties of $Hg^{2+}$, $Hg^p$, and $Hg^0$, studies for the $Hg^0$ removal method should be first taken into account.

Among technologies under development, activated carbon (AC) injection is widely employed as the leading technology for the control of mercury in coal-fired utility plants, because almost all coal-fired power plants are equipped with an ESP or a baghouse.[9−11] However, the AC has limited mercury capture capacity, with carbon/mercury weight ratios of 2843−4361 being common.[12] To reduce the injection rate of AC and improve the efficiency of mercury capture, ACs have been chemically modified, often using oxidizers, such as Br, Cl, and sulfur-containing substances.[10,13−15] These studies showed that chemically modified ACs had a stronger capacity for $Hg^0$ removal. However, obvious disadvantages, such as higher operation expenses, poor capacity, narrow temperature range of application, and slow regeneration and adsorption rates, were identified via this technology, thus restricting their wide application.[9,10,16,17]

As reported, promoting the $Hg^0$ oxidation is another current technology for the control of $Hg^0$, on the basis that $Hg^{2+}$ can be removed through currently available pollution control devices. Recently, some transition-metal oxides, such as $Fe_2O_3$, $V_2O_5$, CuO, $Mn_2O_3$, and $RuO_2$, have been extensively investigated as potential $Hg^0$ oxidation catalysts, and it has been observed that these metal oxides were helpful to the oxidation of $Hg^0$ to $Hg^{2+}$.[18−21] In addition, with the spread of selective catalytic reduction (SCR) installation in coal-fired power plants for NO emission control, the co-benefit effect of the SCR system for oxidizing $Hg^0$ has been widely studied.[22−27] The results showed that commercial SCR catalysts were effective for $Hg^0$ conversion in the flue gas. However, the predictability of the removal extent was unreliable. Moreover, the required operating temperatures for those commercial catalysts applied in industries are typically 300−500 °C, which makes it necessary to locate the SCR unit at the upstream of the denitration setup and/or particulate control device to avoid reheating the flue gas. Unfortunately, the life span of catalysts is shortened because of the chronic exposure to high concentrations of $SO_2$ and ashes. The decomposition of $Hg^{2+}$ (especially $HgCl_2$) is easy to take place at this temperature range.[28] Therefore, it is desirable to develop the low-temperature (80−300 °C) SCR catalysts, which cannot only avoid those problems but also perform higher removal efficiencies for NO and $Hg^0$. Ji et al.[29] found that $MnO_x$ supported on titania was effective for both $Hg^0$ capture and

**Received:** November 8, 2011
**Revised:** February 27, 2012
**Published:** February 29, 2012

  

SCR at 200 °C. Li et al.[30] observed that the CeTi catalyst exhibited high $Hg^0$ oxidation activity from 150 to 250 °C.

In previous works, it was reported that HZSM-5, with higher mechanical strength and chemical and thermal stability, performed high activity on low-temperature SCR of NO.[31−33] In addition, $CeO_2$ was found to have superior activity and stability on $Hg^0$ capture.[34,35] Those results led to a speculation that $Hg^0$ could be efficiently controlled over $CeO_2$/HZSM-5 in SCR systems. Therefore, in this work, $CeO_2$/HZSM-5 was developed and some related experimental parameters, including the $SiO_2/Al_2O_3$ ratio, reaction temperature, $CeO_2$ loading value, and flue gas component, on $Hg^0$ removal efficiencies were evaluated to produce an effective $Hg^0$ emission control strategy for coal-fired power plants.

## 2. MATERIALS AND METHODS

**2.1. Sample Preparation.** Commercially available HZSM-5 (with $SiO_2/Al_2O_3$ ratios of 25, 50, and 100) purchased from NanKai University was used in this study as parental zeolites. Samples of $CeO_2$/HZSM-5 were prepared as follows: First, $Ce(NO_3)_3{\cdot}6H_2O$ was dissolved in deionized water to form the solution. Then, HZSM-5 was added to the solution with stirring in a proportion corresponding to different loading values ($\rho$, where $\rho$ is the mass ratio of $CeO_2$/HZSM-5) varying from 2 to 12 wt %. Third, the samples were dried in an electric blast drying oven at 120 °C for 24 h and then calcined at 450, 550, or 650 °C in air for 5 h. The obtained samples, designated as $\rho$ $CeO_2$/HZSM-5 ($A$)-$T$ (where "$A$" denotes the $SiO_2/Al_2O_3$ ratio and "$T$" denotes the calcination temperature), were crushed and sieved to 40−60 mesh particles for future use. Besides, to investigate the reactivation ability of the samples, the recycling sample was heated in a flow of $N_2$ at 650 °C for 6 h and then cooled to ambient temperature for future use.

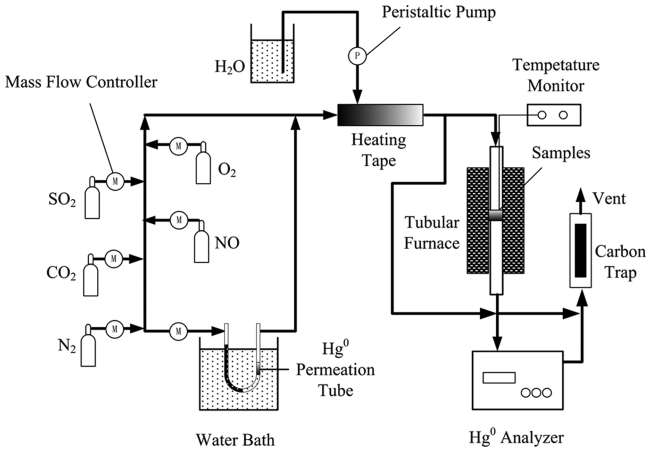


**Figure 1.** Schematic diagram of the experimental setup.

**2.2. Catalytic Test.** A schematic diagram of the experimental setup is shown in Figure 1. The apparatus consisted of a simulated flue gas system, a fixed-bed reactor, and a gas analyzer system. The composition of the basic flue gas included 8% $O_2$, 1000 ppm NO, 1200 ppm $SO_2$, 12% $CO_2$, 10% $H_2O$, and balance gas $N_2$. The $N_2$ flow was divided into two branches: one branch converged with the individual streams of NO, $CO_2$, $SO_2$, $H_2O$, and $O_2$ and formed the main gas flow, and the other branch (150 mL/min) passed through a $Hg^0$ permeation tube (VICI Metronics) and introduced the saturated $Hg^0$ vapor into the reactor. The $Hg^0$ permeation tube was placed in a U-shaped glass tube, which was immersed in a constant temperature water bath to ensure a constant $Hg^0$ permeation rate. The $Hg^0$ concentration in this system was controlled at 20.02 ± 1 $\mu g/m^3$. The total flow was controlled at 0.5 L/min in each experiment, corresponding to a space velocity of about 10 000 $h^{-1}$.

Because quartz had been demonstrated to have good chemical resistance and inertness toward mercury, a quartz tube with an inner diameter of 10 mm held in a vertical position was used as the reactor, which was surrounded by a large tubular furnace, and about 0.1 g of the samples was packed in it. A temperature control device was employed to keep the fixed-bed reactor at the desired temperature. The $Hg^0$ concentration at both the inlet and outlet of the fixed-bed reactor were measured by the $Hg^0$ analyzer. After each analysis, the exhaust gas from the mercury analyzer was introduced into the AC trap before being introduced into the air. During the experiment, the experimental gas first bypassed the quartz tube and was introduced into the catalytic system until the desired inlet mercury concentration had been established for about 20 min. For the whole tests, the $Hg^0$ removal efficiency ($\eta$) was quantified by a comparison between the inlet and outlet $Hg^0$ concentration of the quartz tube. $\eta$ is defined as reaction 1

$$\eta_{Hg^0} = \frac{Hg^0{}_{inlet} - Hg^0{}_{outlet}}{Hg^0{}_{inlet}} \times 100\% \quad (1)$$

where $Hg^0_{in}$ is the inlet $Hg^0$ concentration of the quartz tube and $Hg^0_{out}$ is the outlet $Hg^0$ concentration of the quartz tube.

**2.3. Analytical Methods.** Textural characteristics of the samples were determined by nitrogen adsorption at −196 °C on a Micromeritics ASAP 2010 analyzer. The specific surface area was calculated on the basis of the Brunauer−Emmett−Teller (BET) method. The pore size distribution was characterized using the desorption branches of the $N_2$ adsorption isotherm and the Barret−Joyner−Halenda (BJH) formula. All of the samples were degassed at 120 °C prior to BET measurements. The scanning electron microscopy (SEM) photographs of the samples were obtained by means of JSM-6700F after vacuum plating Au film. X-ray diffraction (XRD) measurements of the samples were carried out with a Rigaku Rotaflex D/Max-C system with Cu K$\alpha$ ($\lambda$ = 0.1543 nm) radiation to determine the crystal species distribution of the sample. The samples were loaded on a sample holder with a depth of 1 mm. Thermogravimetric analysis (TGA; STA-409PC/PG) was used to determine the speciation of mercury deposits on used samples. To promote the experiment so that the capacity of the composite material can be more easily tested, the samples were first exposed to the simulated flue gas with 200 $\mu g/m^3$ $Hg^0$ for about 400 h. For each test, about 10 mg of samples was heated from room temperature to 800 °C at the heating rates of 10 °C/min under a nitrogen atmosphere (>99.99%). The flow rate of $N_2$ was kept at 100 mL/min to ensure an inert atmosphere during the run. During the experiments, the inlet and outlet $Hg^0$ concentrations were measured online by the portable mercury analyzer (model QM201G), which was based on cold-vapor atomic fluorescence spectroscopy. The detection limit was 0.001 $\mu g/m^3$, and the nominal range was 0.01−100 $\mu g/m^3$.

## 3. RESULTS AND DISCUSSION

**3.1. Sample Characteristics.** The BET surface areas and volumes of the parental and modified HZSM-5 are listed in Table 1. It could be observed that the fresh HZSM-5 had the highest BET surface area and the largest pore volume, 340 $m^2/g$ and 0.170 $cm^3/g$, respectively, but they decreased with the increase of the $CeO_2$ loading value. Especially, when the $CeO_2$ loading value reached 12%, the BET surface area sharply reduced to 240.20 $m^2/g$ and the total pore volume reduced to 0.141 $m^3/g$.

The SEM photographs of HZSM-5 and 6% $CeO_2$/HZSM-5 (50)-550 are displayed in Figure 2. As shown in Figure 2a, HZSM-5 was composed of numerous ellipse crystal particles and the average particle size was about 50−200 nm. The surface of HZSM-5 was smooth, and the microcrystal was clear, without any adsorbed particle. When Figure 2b is compared to


dx.doi.org/10.1021/ef201739p | Energy Fuels 2012, 26, 2082−2089

**Table 1. Specific Surface Area and Volume of the Samples**

| samples | BET surface area ($m^2/g$) | total pore volume ($cm^3/g$) |
|---|---|---|
| HZSM-5 | 340.32 | 0.170 |
| 3% $CeO_2$/HZSM-5 (50)-550 | 319.23 | 0.163 |
| 6% $CeO_2$/HZSM-5 (50)-550 | 297.63 | 0.158 |
| 9% $CeO_2$/HZSM-5 (50)-550 | 257.87 | 0.147 |
| 12% $CeO_2$/HZSM-5 (50)-550 | 240.20 | 0.141 |
| first regenerated 6% $CeO_2$/HZSM-5 (50)-550 | 278.58 | 0.151 |
| second regenerated 6% $CeO_2$/HZSM-5 (50)-550 | 275.39 | 0.150 |

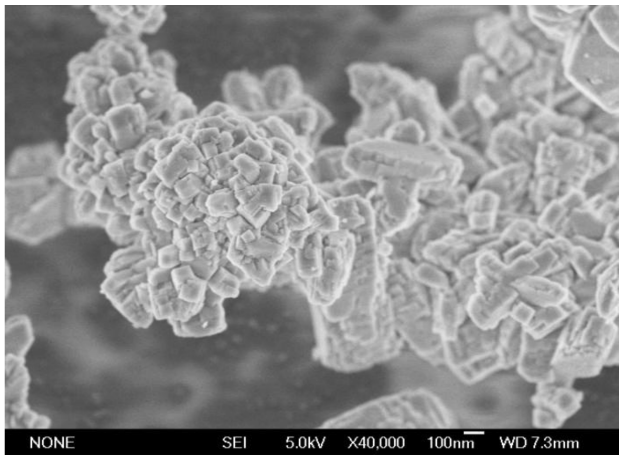


(a)

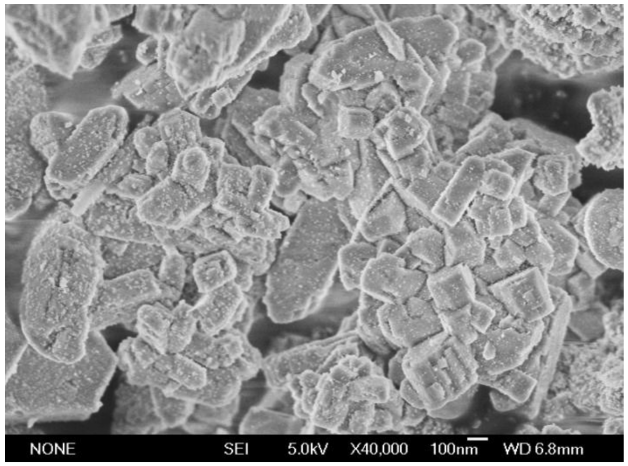


(b)

**Figure 2.** SEM photographs of (a) HZSM-5 zeolite and (b) 6% $CeO_2$/HZSM-5 (50)-550.

Figure 2a, there were more white-circled spots on the surface of $CeO_2$/HZSM-5, which could be ascribed to $CeO_2$ particles. Meanwhile, these particles were widely dispersed on the HZSM-5 surface, and only a few agglomerations existed; however, its particle size was too small to be recognized.

The XRD patterns of HZSM-5 and $CeO_2$/HZSM-5 (50)-550 are shown in Figure 3. The peaks at the ranges of $2\theta = 7-9°$ and $23-25°$ in the XRD pattern were corresponding to the specific peaks of HZSM-5, which could be detected over all of the samples. However, there were no apparent characteristic

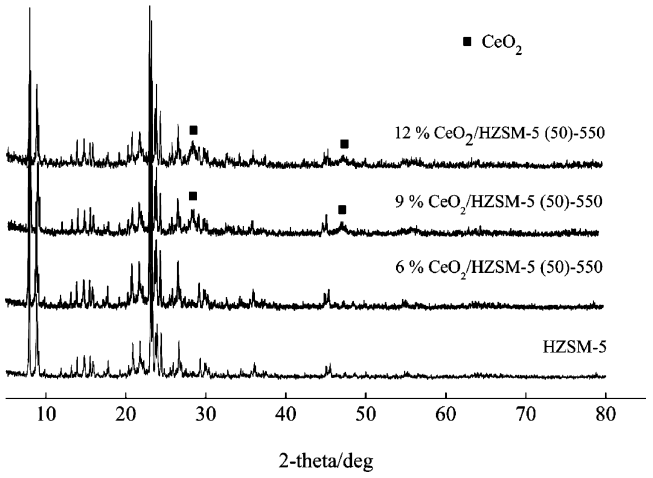


**Figure 3.** XRD patterns of HZSM-5 and $CeO_2$/HZSM-5 (50)-550.

peaks ascribable to $CeO_2$ over 6% $CeO_2$/HZSM-5 (50)-550, which indicated that $CeO_2$ was highly dispersed on the surface of HZSM-5.[36] The result was in accordance with the result of Figure 2b and Table 1. Nevertheless, a weak crystal phase of $CeO_2$ was detected for 9% $CeO_2$/HZSM-5 and 12% $CeO_2$/HZSM-5, powerfully indicating that the surface of HZSM-5 is occupied by $CeO_2$ as the $CeO_2$ loading increases to somewhere between 6 and 9%.

**3.2. Effect of the $SiO_2/Al_2O_3$ Ratio.** The effect of the $SiO_2/Al_2O_3$ ratio on the $Hg^0$ removal efficiency was investigated using 6% $CeO_2$/HZSM-5-550 with the different $SiO_2/Al_2O_3$ ratios (25, 50 and 100) over a range of reaction temperatures (80–320 °C). The experimental results are shown in Figure 4. With the increase of the $SiO_2/Al_2O_3$ ratio,

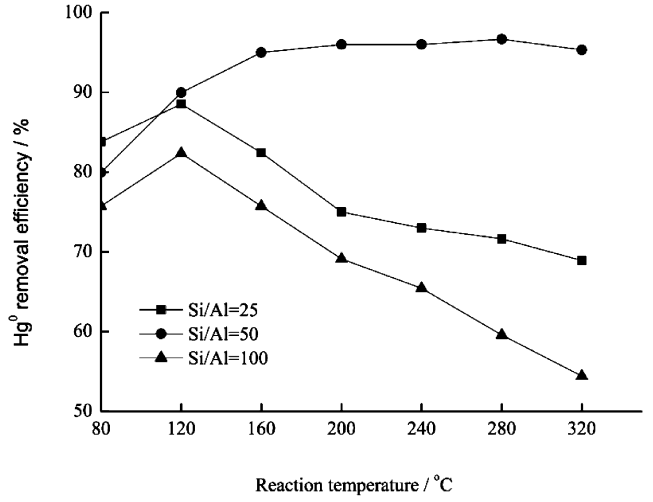


**Figure 4.** Effect of the $SiO_2/Al_2O_3$ ratio on the performance of 6% $CeO_2$/HZSM-5-550.

the activity of 6% $CeO_2$/HZSM-5-550 for the aimed reaction obviously decreased at 80 °C. However, when the reaction temperature increased to 120 °C, the $Hg^0$ removal efficiencies of all samples were enhanced and the efficiency of the sample with the $SiO_2/Al_2O_3$ ratio of 50 was superior to 25. With the continued increase of the temperature to 320 °C, the $Hg^0$ removal efficiencies of 6% $CeO_2$/HZSM-5 (25)-550 and 6% $CeO_2$/HZSM-5 (100)-550 reduced, while the efficiency of 6% $CeO_2$/HZSM-5 (50)-550 changed slightly in this temperature


dx.doi.org/10.1021/ef201739p | Energy Fuels 2012, 26, 2082–2089

scope. This indicated that 6% $CeO_2$/HZSM-5 (50)-550 not only had the wide temperature window but could also offer excellent $Hg^0$ removal efficiency.

**3.3. Effect of the Calcination Temperature.** To further evaluate the activity of this sample, the $Hg^0$ removal efficiencies of 6% $CeO_2$/HZSM-5 (50) calcined at 450, 550, and 650 °C were tested under different reaction temperatures (80−320 °C), and the results are shown in Figure 5. From these results,

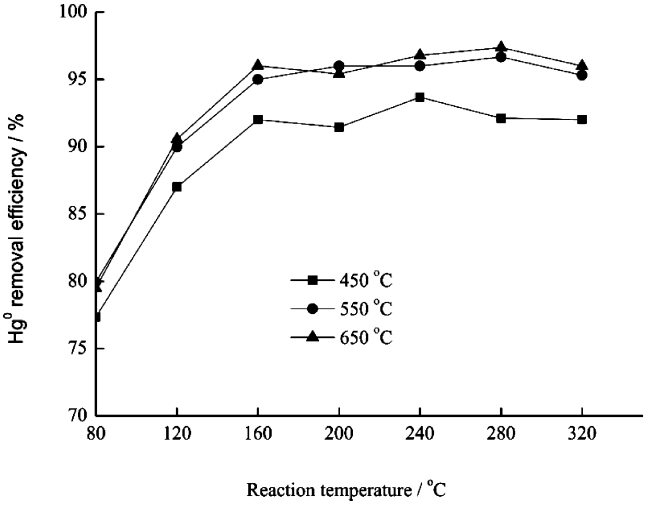


**Figure 5.** Effect of the calcination temperature on the performance of 6% $CeO_2$/HZSM-5 (50).

it could be seen that the conditions of calcinations had an important effect on the performance of the sample. When the calcination temperature changed from 450 to 550 °C, the $Hg^0$ removal efficiency increased an average of 5% in the whole reaction temperature range but no obvious increase was detected when the reaction temperature was increased from 550 to 650 °C. This result illustrated that the decomposition of cerium nitrate on HZSM-5 seemed to be complete when the calcination temperature reached 550 °C. On the basis of the above results, the reasonable calcination temperature was chosen as 550 °C for the fabrication of $CeO_2$/HZSM-5.

**3.4. Effect of the $CeO_2$ Loading Value.** The effects of the $CeO_2$ loading value on $Hg^0$ removal efficiency were studied over 0, 3, 6, 9, and 12% $CeO_2$/HZSM-5 (50)-550 under 200 °C. As shown in Figure 6, the $Hg^0$ removal efficiency of HZSM-5 was noticeably enhanced by $CeO_2$. For example, the $Hg^0$ removal efficiency of HZSM-5 was only 50%, while the minimal $Hg^0$ removal efficiency still had 75% over $CeO_2$-modified HZSM-5. Moreover, the more the loading value of $CeO_2$ was loaded, the higher the $Hg^0$ removal efficiency. However, when the loading value of $CeO_2$ was greater than 6%, correspondingly, the $Hg^0$ removal efficiency would be weakened. From Table 1, it could be found that the surface area of $CeO_2$/HZSM-5 was reduced (about 47 $m^2/g$) with the increase of the loading value from 6 to 9%. This was due to the fact that the existence of agglomerated $CeO_2$ (shown in Figure 3) over the external surface of the samples caused destruction of the thin pore walls and blocking of internal porosity, which affected effective contact between $Hg^0$ and $CeO_2$/HZSM-5 and led to the decrease of the $Hg^0$ removal efficiency.[36,37]

**3.5. Effect of the Flue Gas Components.** To better evaluate the $Hg^0$ removal ability of $CeO_2$/HZSM-5, the effects of individual flue gas components were examined over 6%

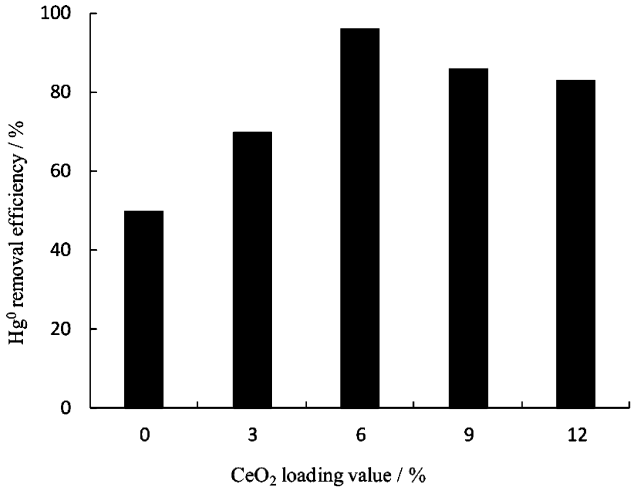


**Figure 6.** Effect of the $CeO_2$ loading value on the performance of $CeO_2$/HZSM-5 (50)-550.

$CeO_2$/HZSM-5 (50)-550 at 200 °C, and the results are illustrated in Figure 7.

Figure 7a shows the effect of different $O_2$ concentrations (0, 5, 8, and 12%) in the flue gas on $Hg^0$ removal efficiency. About 67% $Hg^0$ removal efficiency was achieved in the absence of $O_2$ in the flue gas, but when the $O_2$ concentration was increased to 5%, the $Hg^0$ removal efficiency reached almost 90%. Meanwhile, the $Hg^0$ removal efficiency continued to be enhanced with the rise of the $O_2$ concentration. It indicated that $O_2$ in the flue gas system played a significant role in $Hg^0$ removal over $CeO_2$/HZSM-5. The influences of $SO_2$ on $Hg^0$ removal efficiency of 6% $CeO_2$/HZSM-5 (50)-550 were investigated in the presence of 0−1600 ppm $SO_2$. As depicted in Figure 7b, when the concentration of $SO_2$ was changed from 0 to 800 ppm, the $Hg^0$ removal efficiency of 6% $CeO_2$/HZSM-5 (50)-550 would be increased from 89 to 95.2%. However, as the concentration of $SO_2$ continued to increase, no obvious increase of the $Hg^0$ removal efficiency was detected. The $Hg^0$ removal ability of 6% $CeO_2$/HZSM-5 (50)-550 was studied when 0−1400 ppm NO was individually added into the flue gas, and the results are shown in Figure 7c. The $Hg^0$ removal efficiency of 6% $CeO_2$/HZSM-5 (50)-550 was promoted by NO, and the promotion was proportional to the concentration of NO. Figure 7d shows the effect of $H_2O$ on $Hg^0$ removal efficiency without adding $H_2O$ and with adding 8% $H_2O$ into the experimental flue gas. When 8% $H_2O$ was added into the flue gas, only 82.6% of $Hg^0$ was removed. It indicated that the presence of $H_2O$ restrained the $Hg^0$ removal ability of 6% $CeO_2$/HZSM-5 (50)-550.

**3.6. Reaction Mechanism of the $Hg^0$ Removal.** According to reports, the reaction mechanism of $Hg^0$ removal was attributed to the combined action of physisorption and chemisorption.[34,35,38,39] First, $Hg^0$ in the flue gas collided with the materials and was reversibly adsorbed on the surface of the materials because of the van de Waals force, which ascribed to the physisorption. This physisorption was mainly dependent upon the acid sites of the surface of the sample and would be weaken with the increase of the reaction temperature.[40] Second, the adsorbed $Hg^0$ could be oxidized by some active constituent on the surface of the sample, leading to the formation of new mercury species. This function put down to the chemisorption, which was irreversible and would boost with the increase of the reaction temperature because of the formation of more


dx.doi.org/10.1021/ef201739p | Energy Fuels 2012, 26, 2082−2089

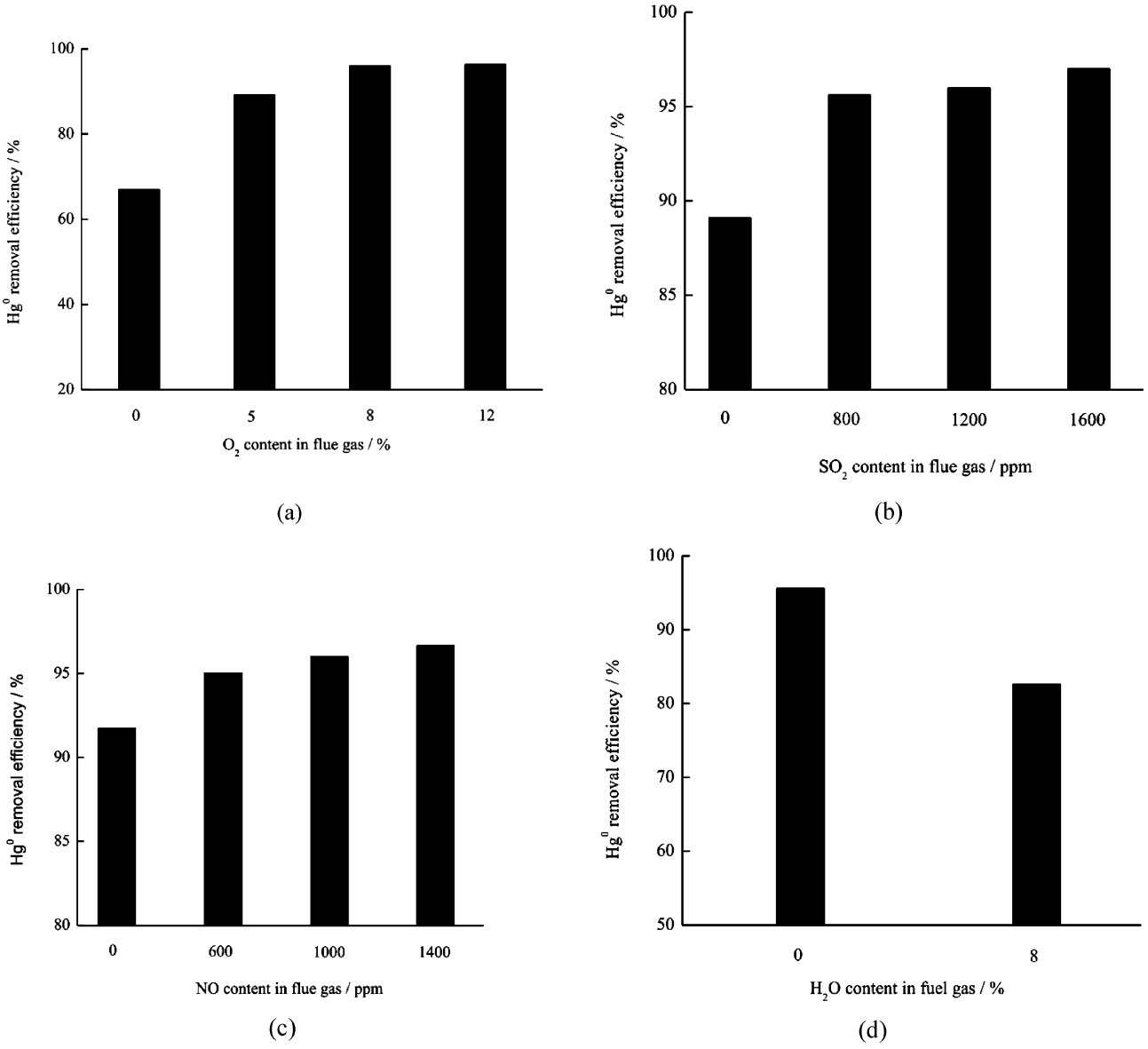


**Figure 7.** Effect of flue gas components on the $Hg^0$ removal efficiency of 6% $CeO_2$/HZSM-5 (50)-550 at 160 °C: (a) $O_2$, (b) $SO_2$, (c) NO, and (d) $H_2O$.

chemical bonds between them.[41] This mechanism could be used to explain that the $Hg^0$ removal efficiency of 6% $CeO_2$/HZSM-5 increased and then decreased with the increase of the reaction temperature in Figure 4. When the reaction temperature increased from 80 to 120 °C, the potentiation of chemisorption was stronger than the inhibition of physisorption, but the contrary was indeed true when the temperature exceeded 120 °C.

Furthermore, $CeO_2$/HZSM-5 with a Si/Al ratio of 25 performs the highest $Hg^0$ removal efficiency at lower temperatures in Figure 4. This was because the acid sites of the $CeO_2$/HZSM-5 surface were attributed to Al in the framework of HZSM-5.[32] $CeO_2$/HZSM-5 with a Si/Al ratio of 25 had more acid sites, which could perform stronger physisorption at a lower temperature (80 °C). However, the $Hg^0$ removal efficiency of $CeO_2$/HZSM-5 (50)-550 was superior to $CeO_2$/HZSM-5 (25)-550 at 120 °C in Figure 4. This was due to the fact that the electrostatic field of HZSM-5 in favor of the redox activity of HZSM-5 would be strengthened with the increase of the Si/Al ratio, which enhanced the chemisorption of the remover.[33] Therefore, the potentiation of chemisorption owing to a higher Si/Al ratio was superior to the inhibition of physisorption. These results further verified the conclusion that the $Hg^0$ remover was attributed to the combined action of physisorption and chemisorption.

To further confirm the mechanism of $Hg^0$ removal over $CeO_2$/HZSM-5, TGAs of recycling 6% $CeO_2$/HZSM-5 were employed, and the results are shown in Figure 8. As shown in Figure 8, there was a quick mass loss as the temperature increases up to 100 °C, which corresponded to the loss of desorbed water. When the weight loss of the samples is compared in the presence and absence of $Hg^0$, the excess weight loss between 50 and 300 °C was attributed to the physical adsorption of mercury, which was often presented as $Hg^0$.[12] The amount of $Hg^0$ present on the sample was about 7 mg/g based on the mass balance calculation. The other excess weight loss between 400 and 600 °C was attributed to chemical adsorption of mercury, which was presented as HgO and/or


dx.doi.org/10.1021/ef201739p | Energy Fuels 2012, 26, 2082–2089

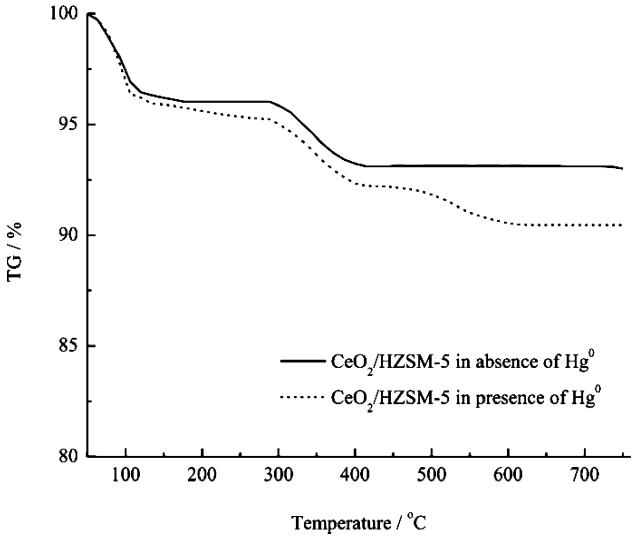


**Figure 8.** TGAs of the samples.

$HgSO_4$, because the thermodecomposition of HgO and $HgSO_4$ often took place in the 430−560 and 500−600 °C temperature intervals, respectively.[28] The amount of $Hg^{2+}$ on the sample was about 17 mg/g. Figure 8 revealed that $Hg^0$ was captured as both $Hg^0$ and $Hg^{2+}$, while the chemisorption was the crucial factor for the $Hg^0$ removal over $CeO_2$/HZSM-5.

It could be seen from Figures 6 and 7a that the presence of $CeO_2$ was favorable for the $Hg^0$ removal of 6% $CeO_2$/HZSM-5 in the presence of $O_2$. Moreover, it had also been proven that lattice oxygen of $CeO_2$ was the most abundant reactive intermediate that could serve as the oxidant of $Hg^0$.[39,30,42] Therefore, it was concluded that the oxidation of $Hg^0$ was attributed to the activity of $CeO_2$. $CeO_2$ has the cubic fluorite structure and typically possesses a relatively high density of oxygen vacancies. On the other hand, the electron structure of Ce is $4f^15d^16s^2$, and its 5d orbit has only one electron, which provides a good electron-transfer orbit. For this reason, $CeO_2$ exhibits an oxygen storage capacity through a facile $Ce^{4+}/Ce^{3+}$ redox cycle and can effectively enhance the oxygen mobility.[35] The appearance of $CeO_2$ on the catalyst surface resulted in more chemisorbed sites, which was probably responsible for the excellent oxidation of the performance of $CeO_2$/HZSM-5 on $Hg^0$. On the other hand, $O_2$ could reoxidize the reduced metal oxides, replenish the lattice oxygen, and hence, maintain the high chemisorbed sites.[42]

Specifically, the reaction mechanism of $Hg^0$ removal by $CeO_2$/HZSM-5 could be explicated as follows:

$$Hg^0_{(g)} + \text{HZSM-5} \leftrightarrow Hg^0_{(ad)} \quad (2)$$

Then, adsorbed $Hg^0$ could be oxidized by $CeO_2$ by a short-range transfer step from HZSM-5 to the $CeO_2$ surface through the following reaction:

$$Hg^0_{(ad)} + 2CeO_2 \rightarrow HgO_{(ad)} + Ce_2O_3 \quad (3)$$

$Ce_2O_3$ generated in reaction 3 could be restored by the following pathway:

$$2Ce_2O_3 + O_2 \rightarrow 4CeO_2 \quad (4)$$

The above results also demonstrated the synergy for $Hg^0$ oxidation when $CeO_2$ and HZSM-5 were combined.

As shown in Figure 7, when adding NO and $SO_2$ into the flue gas, the $Hg^0$ removal efficiency of $CeO_2$/HZSM-5 would be promoted. This trend agreed with the results obtained by other researchers.[23,29,30,43] It could be attributed to the fact that $CeO_2$ was more active for NO and $SO_2$ oxidation as follows:

$$2NO_{(g)} + O_2 \xrightarrow{CeO_2} 2NO2_{(ad)} \quad (5)$$

$$2SO_2{}_{(g)} + O_2 \xrightarrow{CeO_2} 2SO_3{}_{(ad)} \quad (6)$$

Moreover, $CeO_2$ was favorable for the storage of $NO_2$ and $SO_3$, which had a promoted effect on the oxidation of $Hg^0$ by the following pathway:[44]

$$NO_2{}_{(ad)} + Hg_{(ad)} \rightarrow NO + HgO_{(ad)} \quad (7)$$

$$SO_3{}_{(ad)} + Hg_{(ad)} \rightarrow SO_2 + HgO_{(ad)} \quad (8)$$

$$SO_3{}_{(ad)} + HgO_{(ad)} \rightarrow HgSO_4{}_{(ad)} \quad (9)$$

Additionally, the result was somewhat different from that reported by Wen et al.,[36] who reported that the presence of $SO_2$ could inhibit the $Hg^0$ removal. Likely, this difference resulted from their higher operation temperature (>300 °C). When the temperature exceeds 300 °C, excessive $CeO_2$ would react with $SO_2$ and $O_2$, forming $Ce(SO_4)_2$. Generated $Ce(SO_4)_2$ covers the surface of HZSM-5 and blocks its pores, preventing $Hg^0$ from contacting $CeO_2$.

The inhibitory effects of $H_2O$ for $Hg^0$ removal could be explained by the competitive adsorption of water vapor with $Hg^0$, which was reported in other studies.[36,42,43] Meanwhile, $H_2O$ was not necessarily monolayer adsorption. It could fill pores and, hence, block adsorption of other components.[45] Furthermore, adsorbed $H_2O$ could react with $SO_3$ to form $H_2SO_4$, which could destroy the framework of HZSM-5. As a result, the $Hg^0$ removal ability of $CeO_2$/HZSM-5 was weakened in humid conditions in this work.

**3.7. Removal Stability and Recyclability.** The $Hg^0$ removal stabilities of 6% $CeO_2$/HZSM-5 (50)-550 and regenerated 6% $CeO_2$/HZSM-5 (50)-550 were tested under 200 °C, and the experimental results are shown in Figure 9. It was remarkable that the activity of 6% $CeO_2$/HZSM-5 (50)-550 performed good stability and showed higher $Hg^0$ removal

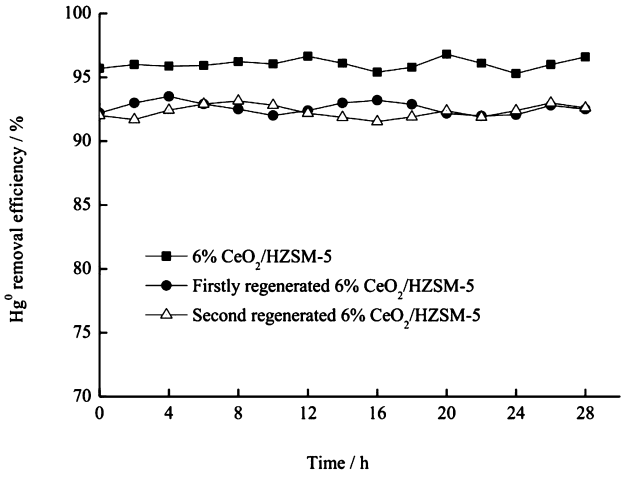


**Figure 9.** $Hg^0$ removal efficiencies of fresh 6% $CeO_2$/HZSM-5 and regenerated 6% $CeO_2$/HZSM-5.


dx.doi.org/10.1021/ef201739p | Energy Fuels 2012, 26, 2082−2089

efficiency of 95% in 30 h. It indicated that $CeO_2$/HZSM-5 could be desirable for $Hg^0$ removal in industrial applications. Furthermore, it could be seen that the $Hg^0$ removal efficiency of regenerated $CeO_2$/HZSM-5 was lower than that of fresh 6% $CeO_2$/HZSM-5. This might be due to the decrease of the surface and volume, which could be seen from Table 1. Nevertheless, the $Hg^0$ removal efficiency of first and second regenerated $CeO_2$/HZSM-5 was about 92% and remained stable for 30 h. Therefore, it was concluded that $CeO_2$/HZSM-5 was recyclable and suitable for reuse.

## 4. CONCLUSION

In this paper, the $Hg^0$ removal ability of $CeO_2$/HZSM-5 was investigated in a lab-scale fixed-bed system. Results showed that $CeO_2$ significantly enhanced the $Hg^0$ removal ability of HZSM-5. Especially when $CeO_2$/HZSM-5 (50) was calcined above 550 °C, the $Hg^0$ removal efficiency went to a maximum at 200 °C, up to about 96%. Additionally, the $Hg^0$ removal efficiency was found to be significantly affected by the flue gas components. Both NO and $SO_2$ promoted the $Hg^0$ removal in the presence of $O_2$. However, when $H_2O$ was added into the reactant stream, the $Hg^0$ removal ability of the sample had a slight decline. In comparison to other SCR catalysts, $CeO_2$/HZSM-5 performed stronger $Hg^0$ removal ability at low reaction temperatures (<300 °C). In addition, it was also found in previous works that HZSM-5 and $CeO_2$ were highly active for low-temperature SCR of NO. Thus, it is concluded that this material may be used in some SCR systems that are downstream of the particulate control device (hot-side ESP), where it can avoid a high concentration of ashes in the flue gas. Moreover, the regeneration of $CeO_2$/HZSM-5 was easy. After regeneration, the $Hg^0$ removal efficiency of $CeO_2$/HZSM-5 was still kept basically stable, with high efficiency for 30 h. Therefore, it indicated that $CeO_2$/HZSM-5 was recyclable and suitable for reuse on $Hg^0$ removal from flue gas.

## ■ AUTHOR INFORMATION

### Corresponding Author

*Telephone/Fax: +86-731-88649216. E-mail: ctli3@yahoo.com.

### Notes

The authors declare no competing financial interest.

## ■ ACKNOWLEDGMENTS

The authors gratefully acknowledge the financial support of the National High Technology Research and Development Program of China (863 Program) (2011AA060803), the National Natural Science Foundation Project of China (NSFC-51108169), and the Scientific and Technological Major Special Project of Hunan Province in China (2010XK6003).

## ■ REFERENCES

(1) Lindberg, S. E.; Stratton, W. J. *Environ. Sci. Technol.* **1998**, *32*, 49−57.
(2) Vandal, G. M.; Fitzgerald, W. F. *Nature* **1993**, *362*, 621−623.
(3) Dastoora, A. P.; Larocpue, Y. *Atmos. Environ.* **2004**, *38*, 147−161.
(4) Brown, T. D.; Smith, D. N.; Hargis, R. A. *Air Waste Manage. Assoc.* **1999**, *49*, 628−640.
(5) Pacyna, E. G.; Pacyna, J. M.; Steenhuisen, F.; Wilson, S. *Atmos. Environ.* **2006**, *40*, 4048−4063.
(6) Wu, Y.; Wang, S. X.; Streets, D. G. *Environ. Sci. Technol.* **2006**, *40*, 5312−5318.
(7) Skodras, G.; Diamantopoulou, Ir.; Pantoleontoc, G.; Sakellaropoulos, G. P. *J. Hazard. Mater.* **2008**, *158*, 1−13.
(8) Wang, Y. J.; Duan, Y. F.; Yang, L. G.; Zhao, C. S.; Shen, X. L. *Fuel Process. Technol.* **2009**, *90*, 643−651.
(9) Liu, Y.; Kelly, D.; Yang, H. Q.; Lin, C.; Kuznicki, S. M.; Xu, Z. H. *Environ. Sci. Technol.* **2008**, *42*, 6205−6210.
(10) Jones, A. P.; Hoffmann, J. W.; Smith, D. N.; Feeley, T. J.; Murphy, J. T. *Environ. Sci. Technol.* **2007**, *41*, 1365−1371.
(11) Huggins, F. E.; Yapa, N.; Huffman, G. P.; Senior, C. L. *Fuel Process. Technol.* **2003**, *82*, 167−196.
(12) Pitoniak, E.; Wu, C. Y.; Mazyck, D. W.; Powers, K. W.; Sigmund, W. *Environ. Sci. Technol.* **2005**, *39*, 1269−1274.
(13) Feng, W. G.; Borguet, E.; Vidic, R. D. *Carbon* **2006**, *44*, 2990−2997.
(14) Hu, C. X.; Zhou, J. S.; He, S.; Luo, Z. Y.; Cen, K. F. *Fuel Process. Technol.* **2009**, *90*, 812−817.
(15) Liu, S. H.; Yan, N. Q.; Liu, Z. R.; Qu, Z.; Wang, H. P.; Chang, S. G.; Miller, C. *Environ. Sci. Technol.* **2007**, *41*, 1405−1412.
(16) Tong, S. T.; Fan, M. X.; Mao, L.; Jia, C. Q. *Environ. Sci. Technol.* **2011**, *45*, 7416−7421.
(17) Wu, S. J.; Uddin, M. A.; Sasaoka, E. *Fuel* **2006**, *85*, 213−218.
(18) Dunham, G.; Dewall, R.; Senior, C. *Fuel Process. Technol.* **2003**, *82*, 197−213.
(19) Kamata, H.; Ueno, S. I.; Sato, N.; Naito, T. *Fuel Process. Technol.* **2009**, *90*, 947−951.
(20) Li, J. F.; Yan, N. Q.; Qu, Z.; Qiao, S. H.; Yang, S. J.; Guo, Y. F.; Liu, P.; Jia, J. P. *Environ. Sci. Technol.* **2010**, *44*, 426−431.
(21) Yan, N. Q.; Chen, W. M.; Chen, J.; Qu, Z.; Guo, Y. F.; Yang, S. J.; Jia, J. P. *Environ. Sci. Technol.* **2011**, *45*, 5725−5730.
(22) Eswaran, S.; Stenger, H. G. *Energy Fuels* **2005**, *19*, 2328−2334.
(23) Li, Y.; Murphy, P. D.; Wu, C. Y.; Powers, K. W.; Bonzongo, J. C. *Environ. Sci. Technol.* **2008**, *42*, 5304−5309.
(24) Kamata, H.; Ueno, S. I.; Naito, T.; Yukimura, A. *Ind. Eng. Chem. Res.* **2008**, *47*, 8136−8141.
(25) Chen, L.; Li, J. H.; Ge, M. F. *J. Phys. Chem. C* **2009**, *113*, 21177−21184.
(26) Mei, Z. J.; Shen, Z. M.; Mei, Z. Y.; Zhang, Y. J.; Xiang, F.; Chen, J. P.; Wang, W. H. *Appl. Catal., B* **2008**, *78*, 112−119.
(27) Straube, S.; Hahn, T.; Koeser, H. *Appl. Catal., B* **2008**, *79*, 286−295.
(28) Lopez-Anton, M.; Yuan, Y.; Perry, R.; Maroto-Valer, M. *Fuel* **2010**, *89*, 629−634.
(29) Ji, L.; Sreekanth, P. M.; Smirniotis, P. G.; Thiel, S. W.; Pinto, N. G. *Energy Fuels* **2008**, *22*, 2299−2306.
(30) Li, H. L.; Wu, C. Y.; Li, Y.; Zhang, J. Y. *Environ. Sci. Technol.* **2011**, *45*, 7394−7400.
(31) Ding, Y. M.; Li, C. T.; Zeng, G. M.; Lu, P. *Acta Sci. Circumstantiae* **2009**, *29*, 2572−2577.
(32) Wang, C.; Wang, X. P.; Xing, N.; Yu, Q.; Wang, Y. J. *Appl. Catal., A* **2008**, *334*, 137−146.
(33) Wang, X. P.; Yu, S. S.; Yang, H. L.; Zhang, S. X. *Appl. Catal., B* **2007**, *71*, 246−253.
(34) Tian, L. H.; Li, C. T.; Li, Q.; Zeng, G. M. *Fuel* **2009**, *88*, 1687−1691.
(35) Lu, P.; Li, C. T.; Zeng, G. M. *Appl. Catal., B* **2010**, *96*, 157−161.
(36) Wen, X. Y.; Li, C. T.; Fan, X. P.; Gao, H. L.; Zhang, W. *Energy Fuels* **2011**, *25*, 2939−2944.
(37) Xie, Y. C.; Tang, Y. Q. *Adv. Catal.* **1990**, *37*, 1−43.
(38) Graydon, J. W.; Zhang, X. Z.; Kirk, D. W.; Jia, C. Q. *J. Hazard. Mater.* **2009**, *168*, 978−982.
(39) Fan, X. P.; Li, C. T.; Zeng, G. M.; Gao, Z.; Chen, L. *Energy Fuels* **2010**, *24*, 4250−4254.
(40) Li, Y. H.; Lee, C. W.; Gullett, B. K. *Fuel* **2003**, *82*, 451−457.
(41) Zeng, H. C.; Jin, F.; Guo, J. *Fuel* **2004**, *83*, 143−146.
(42) Gao, X.; Jiang, Y.; Zhong, Y.; Luo, Z.; Cen, K. *J. Hazard. Mater.* **2010**, *174*, 734−739.
(43) Li, Y.; Murphy, P.; Wu, C. Y. *Fuel Process. Technol.* **2008**, *89*, 567−573.
(44) Liese, T.; Loffler, E.; Grunert, W. *J. Catal.* **2001**, *197*, 123−130.

(45) Casapu, M.; Krocher, O.; Elsener, M. *Appl. Catal., B* **2009**, *88*, 413−419.